Contribution from the School of Chemistry,
The University, Leeds LS2 9JT, U.K.

# Electronic Spectra, Formation Constants, and Geometries of $HgX_3^-$ in Methanol

Trevor R. Griffiths* and Richard A. Anderson

*Received April 4, 1990*

The electronic absorption spectra, in the ultraviolet region, of $HgX_3^-$ (X = Cl, Br, or I) in methanol have for the first time been obtained, by computer techniques, free from any contributions of $HgX_2$ or $HgX_4^{2-}$. Four different and independent methods are described and evaluated. Where the desired spectrum is completely hidden below other bands, here for $HgBr_3^-$ and $HgCl_3^-$, a combination of two methods is needed. Additional tests validated the computed spectra. From these spectra, the stepwise formation constant $K_3$ was computed and found independent of ionic strength at low concentrations. The infinite dilution values are log $K_3(HgCl_3^-) = 1.28 \pm 0.01$, log $K_3(HgBr_3^-) = 3.08 \pm 0.08$, and log $K_3(HgI_3^-) = 5.26 \pm 0.02$. The spectra of $HgX_3^-$ were resolved into their component Gaussian bands and the transitions identified and assigned. This permitted the identification of $HgCl_3^-$ as planar, with $D_{3h}$ symmetry, and $HgI_3^-$ as pyramidal, with $C_{3v}$ symmetry, which suggests that the solvated species are trigonal-bipyramidal and tetrahedral, respectively. The spectrum of $HgBr_3^-$ appears to show features of both symmetries but is here concluded to be closer to pyramidal geometry. Comparisons are made with the structures of $HgX_3^-$ species obtained in dipolar aprotic solvents by other techniques.

## Introduction

The formation of the trihalogeno complex anions of mercury(II), $HgX_3^-$ (X = I, Br, or Cl), occurs readily in dipolar aprotic solvents,[1-6] and generally complete conversion from $HgX_2$ occurs at, or just above, an X/Hg mole ratio of 3. In protic solvents, such as water, much higher ratios are required, and $HgX_4^{2-}$ forms before much $HgX_2$ has reacted to become $HgX_3^-$. From such mixtures we have initially reported[7] the complete electronic absorption spectra of $HgI_3^-$, $HgBr_3^-$, and $HgCl_3^-$ in water and deduced from the resolved spectra that $HgI_3^-$ was pyramidal, but with one coordinated water molecule, giving a near-tetrahedral coordination of mercury, and that $HgCl_3^-$ was planar, but solvated with two water molecules and thus a trigonal-bipyramidal species: $HgBr_3^-$ had intermediate symmetry, but probably was closer in structure to $HgI_3^-$. These structures have also been found by Raman studies in dipolar aprotic solvents,[1,2] but in water Delwaulle[8,9] could only detect some weak lines attributable to $HgX_3^-$ in the presence of the very strong lines of the symmetrical $HgX_4^{2-}$ species. Surprisingly, this work has not been repeated by using laser instrumentation. Sandström and Johansson[10] have made X-ray diffraction studies of, they claim, $HgI_3^-$ and $HgBr_3^-$ in water and report pyramidal structures with one coordinated water molecule. However, the high concentrations and mole ratios they use would also produce tetrahedral $HgX_4^{2-}$ species, and an average separation between species of around one water molecule diameter, and hence possible distortions from regular tetrahedral symmetry. The absorption spectrum of $HgI_3^-$ has been recorded[11] in methanol and ethanol, as part of an investigation of $QHgI_3$ and $Q_2HgI_4$ (Q = $Me_4P^+$ or PyH) in these solvents, but the electronic absorption spectra of $HgBr_3^-$ and $HgCl_3^-$ has not previously been measured in nonaqueous solvents.

This paper describes the electronic absorption spectra of solutions of $HgX_2$ in methanol with added $X^-$ and the various procedures for extracting the spectra of $HgX_3^-$ free from the accompanying contributions of $HgX_2$ and/or $HgX_4^{2-}$, as the procedures were not given in our original preliminary account.[7] From these spectra the stepwise formation constant, $K_3$, for $HgX_3^-$ can be calculated as a function of the ionic strength of the medium. The spectra are also resolved into Gaussian bands and their structure in solution deduced therefrom.

## Experimental Section

**Spectroscopic Measurements.** Spectra were recorded on an Applied Physics Cary 14H spectrophotometer, modified to yield spectra in digitized form on paper tape. Details of the system have been published.[12] Thermostatable cell holders were used, and the water circulated from a thermostat bath maintained the solutions in the cells at 20 ± 0.1 °C.

**Chemicals and Solution Preparation.** All chemicals were of the highest purity, thoroughly dried, and stored in a vacuum desiccator: methanol was spectrograde. All the mercury(II) halides are readily soluble in methanol, and solutions were stable. For solutions requiring very high molarities of alkali-metal halide, the alkali-metal halide was weighed directly in a flask, the required amount of mercury(II) halide solution added, and the solution made up to volume.

**Computing Procedures.** The pen noise inherent in spectroscopic measurements was reduced by mathematical smoothing[13,14] of the digitized spectra, recorded at 1-nm intervals, using a five-point smoothing convolute.

The derivatives of observed and calculated spectra were obtained by using the convolution procedure of Savitsky and Golay.[13,14] This yielded the transition energies of the component bands in a spectrum.

For resolving the spectra of the various $HgX_3^-$ species into their component bands, the conventional least-squares fitting method requires an assumption concerning the type of band distribution involved. For the intramolecular charge-transfer transitions described here, the commonly employed Gaussian function was found most suitable. The program was based on the least-squares minimization procedure of Fletcher and Powell[15] and included matrix inversion[16] to increase the rate of convergence of fit.

**Calculation of Spectra.** The reaction of mercury(II) halides with added halide proceed stepwise, viz.

$$HgX_2 + X^- \rightleftharpoons HgX_3^- \quad (1)$$

$$HgX_3^- + X^- \rightleftharpoons HgX_4^{2-} \quad (2)$$

The tetrahalogeno species begins to form before all the dihalide is converted to the trihalogeno species.[17,18] A steady change in the spectra occurs as halide is added until the spectrum of $HgX_4^{2-}$ only is observed: the spectrum of $HgX_3^-$ cannot be observed free of contributions due to either the di- or the tetrahalide. Here, general methods, some in combination, have been derived and examined in order (in principle) to calculate $HgX_3^-$ from both of the above systems, and we therefore also discuss their various merits.

(1) Waters, D. N.; Kantarci, Z. *J. Raman Spectrosc.* **1977**, *6*, 251.
(2) Waters, D. N.; Kantarci, Z.; Rahman, N. N. *J. Raman Spectrosc.* **1978**, *7*, 288.
(3) Hooper, M. A.; James, D. W. *Aust. J. Chem.* **1971**, *24*, 1345.
(4) Barr, R. M.; Goldstein, M. *J. Chem. Soc., Dalton Trans.* **1974**, 1180.
(5) Sandström, M. *Acta Chem. Scand.* **1977**, *A31*, 141.
(6) Gaizer, F.; Johansson, G. *Acta Chem. Scand.* **1968**, *22*, 3013.
(7) Griffiths, T. R.; Anderson, R. A. *J. Chem. Soc., Chem. Commun.* **1979**, 61.
(8) Delwaulle, M. L. *Spectrochim. Acta Suppl.* **1957**, 565.
(9) Delwaulle, M. L. *Bull. Soc. Chim. Fr.* **1955**, 1294 and references therein.
(10) Sandström, M.; Johansson, G. *Acta Chem. Scand.* **1977**, *A31*, 132.
(11) Deacon, G. B.; West, B. O. *J. Chem. Soc.* **1961**, 3929.
(12) Griffiths, T. R.; Anderson, R. A. *J. Chem. Soc., Dalton Trans.* **1980**, 205.
(13) Savitsky, A.; Golay, M. J. E. *Anal. Chem.* **1964**, *36*, 1627.
(14) Steinier, J.; Termonia, Y.; Deltour, J. *Anal. Chem.* **1972**, *44*, 1906.
(15) Fletcher, R.; Powell, M. J. D. *Comput. J.* **1963**, *6*, 163.
(16) Busing, W. R.; Levy, H. A. *Comm. Assoc. Comput. Mach.* **1970**, *6*, 445.
(17) Sillén, L. G. *Acta Chem. Scand.* **1949**, *3*, 539 and references therein.
(18) Marcus, Y. *Acta Chem. Scand.* **1957**, *11*, 329, 599, 610, 811.

0020-1669/91/1330-1912$02.50/0 

**Use of Known Formation Constants.** For equilibrium 1, upon application of Beer's law and the law of mass action, it may be shown that, at any given wavelength

$$A/M = (\epsilon_a + K_3X\epsilon_b)/(1 + K_3X) \quad (3)$$

where $A$ is the observed absorbance, $M$ is the total molar concentration of metal, $X$ is the free ligand concentration, $K_3$ is the formation constant for $HgX_3^-$ (eq 1), and $\epsilon_a$ and $\epsilon_b$ are the molar absorbances of $HgX_2$ and $HgX_3^-$, respectively. All but $K_3$ and $\epsilon_b$ are experimentally observable. Thus by substitution of known values of $K_3$ into eq 3 the molar absorbance of $HgX_3^-$, as a function of wavelength, i.e. the spectrum of $HgX_3^-$, may be found. This method requires an accurate knowledge of the three $HgX_3^-$ equilibrium constants and that the experimental conditions be exactly the same as those used in the determination of the equilibrium constant.

This method may be extended to utilize the observable spectrum of $HgX_4^{2-}$ by means of the comparable equation, viz.

$$A/M = (\epsilon_b + K_4X\epsilon_c)/(1 + K_4X) \quad (4)$$

where $\epsilon_c$ is the molar absorbance of $HgX_4^{2-}$ and $K_4$ the formation constant for $HgX_4^{2-}$ (eq 2). With the three mercury halides in equilibrium, $\epsilon_b$ (for $HgX_3^-$) may be derived from

$$A/M = (\epsilon_a + K_3X\epsilon_b + K_3K_4X^2\epsilon_c)/(1 + K_3X + K_3K_4X^2) \quad (5)$$

but with less accuracy, due to the increased number of parameters. We have shown earlier[19] that the stability constants for $HgX_3^-$ and $HgX_4^{2-}$ are dependent on ionic strength. In our experiments here, the ionic strength was not normally kept constant, as halide was progressively added to $HgX_2$: it was thus not appropriate in this study to use literature stability constants in the above equations with our molar absorbance data for $HgX_2$ and $HgX_4^{2-}$.

**Least-Squares Method.** Equation 3 may be rearranged to give

$$A' = -(1/K_3)(A' - \epsilon_a)/X + \epsilon_b \quad (6)$$

where $A'$ is the molar absorbance of the solution. With this linear equation, at any given wavelength, for a series of solutions with different ligand concentrations, a least-squares procedure may be applied to yield values of $K_3$ and $\epsilon_b$. Repeating this at all recorded wavelengths will, in principle, yield the entire spectrum of $HgX_3^-$. When tested, this method was here found to be very sensitive to the value of the free ligand concentration. Also, the calculated $K$ values varied widely with wavelength, and hence the spectrum of $HgX_3^-$ thus derived was not meaningful. It would further seem natural that at very low ionic strengths, with a chosen value of $K_3$, the spectrum of $HgX_3^-$ could be calculated directly, using eq 6. Unfortunately, the mercury–halide system did not give identical calculated spectra, as the added halide concentration was steadily increased. This probably arises because the calculation involves a difference (which could be close to noise levels) divided by a small number. At present we therefore do not fully understand these anomalies, despite detailed investigation, and thus would wish to alert others to this variance between principle and practice.

**Comparative Absorbance Plots.** A graphical approach may be used. Comparative absorbance plots of $A'$ vs $(A' - \epsilon_a)/X$, at various wavelengths, will have a slope of $-1/K_3$ and the intercept will be at $\epsilon_b$. Although time consuming and impractical for large numbers of wavelengths, it was useful in that $K_3$ was readily determined and an accurate value for $\epsilon_b$ at any given wavelength could be found for use in the reference-point method (described below).

Equation 4 may be treated similarly to yield the spectrum of $HgX_3^-$, by utilizing the spectrum of $HgX_4^{2-}$.

Since eq 5 is nonlinear with respect to the unknowns $\epsilon_b$, $K_3$, and $K_4$ (with three species in equilibrium), a graphical approach is not applicable under these conditions. However, a least-squares minimization may be applied to such spectra obtained as a function of ligand concentration.

**Reference-Point Method.** For a system containing two absorbing species, A and B, in equilibrium, the molar absorbance at any given wavelength of the solution is given by $\epsilon_d = f_a\epsilon_a + f_b\epsilon_b$, a variant of Beer's Law, where $\epsilon_d$ is the molar absorbance of the solution, $\epsilon_a$ and $\epsilon_b$ are the molar absorbances and $f_a$ and $f_b$ are the mole fractions of A and B, respectively, and further $f_a + f_b = 1$. Upon employing solutions of different relative compositions, we can obtain the molar absorbance of $HgX_3^-$ as

$$\epsilon(HgX_3^-) = \beta(\epsilon_d - \epsilon(HgX_2)) + \epsilon_d \quad (7)$$

The term $\beta = f_a/f_b$, the ratio of the mole fractions of the $HgX_2$ and $HgX_3^-$ species in the sample solution, and $\beta$ may be adjusted to yield any required value of $\epsilon(HgX_3^-)$ at the chosen wavelength. This value of $\beta$ is then used to calculate the absorbance of $HgX_3^-$ at all wavelengths, i.e. the spectrum of $HgX_3^-$, by using a simple iterative computer program.

This method of calculating spectra requires a knowledge of the molar absorbance of $HgX_3^-$ at a given reference wavelength. This may be obtained by one (or more) of five different methods.

(1) Known formation constants, such as those derived from eq 3 or 4 (or, in principle, eq 5), may be used. With our data, the reference-point absorbance had too large an error to yield acceptable spectra for $HgX_3^-$.

(2) Using the least-squares method gives the absorbance at a given wavelength and the formation constant simultaneously but, as indicated above, is not currently recommended.

(3) Comparative absorbance plots yield reference-point absorbances at given wavelengths that compare well with those obtained independently by other methods.

(4) The spectra of solutions of $HgX_2$, as halide is added, will show initially the formation of $HgX_3^-$ and then $HgX_4^{2-}$. Only if the spectrum of $HgX_3^-$ differs considerably from that of $HgX_4^{2-}$, the case for the mercury(II)–iodide system, may the change with added halide be extrapolated to give the molar absorbance of $HgX_3^-$.

(5) When a set of spectra contain one (or more) isosbestic point, this implies that only two species are in equilibrium, and the total mercury(II) concentration is constant.[20,21] Such solutions may contain $HgX_2$ and $HgX_3^-$, or $HgX_3^-$ and $HgX_4^{2-}$, and the molar absorbance of $HgX_3^-$ at the isosbestic point wavelength is thus accurately defined. However, the $HgX_2$ spectrum cannot be used as the reference spectrum, in eq 7, with the isosbestic point(s) as the reference-point absorbance(s) for the $HgX_2 \rightleftharpoons HgX_3^-$ equilibrium, in the calculation of the spectrum of $HgX_3^-$, as the mathematics now involves division by zero. But the isosbestic points formed in the second equilibrium, $HgX_4^{2-}$, are valid as reference points (and vice versa). In practice, only the iodo system contained clearly defined isosbestic points, and the calculated spectrum of $HgI_3^-$ was noisy, unless the original sample spectrum was carefully smoothed. An added complication with the mercury(II) complexes arises because the complexing halide ligand partially absorbs in the spectral region of interest, and this must be accurately computed and subtracted before true molar absorbances of $HgX_3^-$ can be obtained in the overlap region. This iterative procedure is now described.

**Halide Imbalance.** The iodide ion, with a strong absorbance peak in methanol at 218 nm, overlaps most with the spectra of the iodo mercury(II) species. When the various solutions were being prepared, equal quantities of alkali-metal halide were added to the sample and reference solutions. In the former, some free halide, the amount as yet unknown, reacted with $HgX_2$. The reference solution thus had a net excess free halide absorbance compared with that of the sample solution, and, for the iodide, this effectively reduced the true absorbance below 250 nm.

The compensation procedure was as follows. The $HgI_3^-$ spectrum was calculated over the whole wavelength employed, and from this the concentration of $HgI_3^-$ (apparently) present was obtained. The concentration of free iodide ions was found by difference, the absorbance imbalance of the original sample spectrum then calculated, and a new corrected sample spectrum derived. This process was repeated until the difference between successively amended spectra (below 250 nm) was less than a predetermined amount (normally <0.01%). The set of corrected spectra now exhibited two new isosbestic points in place of the original one.

In the case of reference spectra containing chloride and bromide ions, the above procedure may be applied, and for our mercury(II) complexes the imbalance contribution in the far ultraviolet was tested but not found significant enough to warrant its implementation.

**Calculation of Formation Constants $K_3$.** We recently described a new technique for calculating formation constants that uses complete spectra,[19] which eliminates the above-mentioned problem that these constants are very dependent on the values of the molar absorbance values used in eqs 3–5. Since the absorbance $A$ of a multicomponent system is the sum of the products of the molar concentration and molar absorbance of the species present, at all wavelengths, then if $A$ is measured for $n$ different wavelengths, $n$ linear equations of $i$ unknowns may be derived. For $n \gg i$, these linear equations may be accurately solved for $c_i$, the concentrations of the species present, by multiple linear regression analysis. The program gave the required concentrations, with their standard error and various parameters indicating the accuracy of the main computation and the precision of the fitted data. These latter included the residual and regression sum of squares, $F$ ratio, multiple correlation coefficient, and degrees of freedom of the $F$ ratio, together with a table of residuals and standardized residuals. The stability constants, with their standard error,

(19) Griffiths, T. R.; Anderson, R. A. *J. Chem. Soc., Faraday Trans. 1* **1984**, *80*, 2361.

(20) Chylewski, C. *Angew. Chem., Int. Ed. Engl.* **1971**, *10*, 195.

(21) Brynstad, J.; Boston, C. R.; Smith, G. P. *J. Chem. Phys.* **1967**, *47*, 3179.

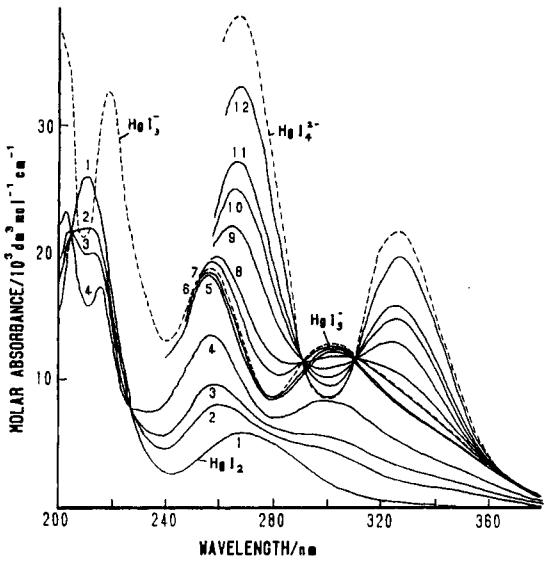


**Figure 1.** Ultraviolet absorption spectra changes obtained upon addition of iodide to $HgI_2$ ($6.7 \times 10^{-5}$ mol dm$^{-3}$) in methanol at 20 °C. Iodide/mercury mole ratios ($R$) are, progressively (1) 2.0 ($HgI_2$), (2) 2.2, (3) 2.3, (4) 2.4, (5), 2.8, (6) 8, (7) 80, (8) 1000, (9) 2000, (10) 3000, (11) 4000, and (12) 60 000.

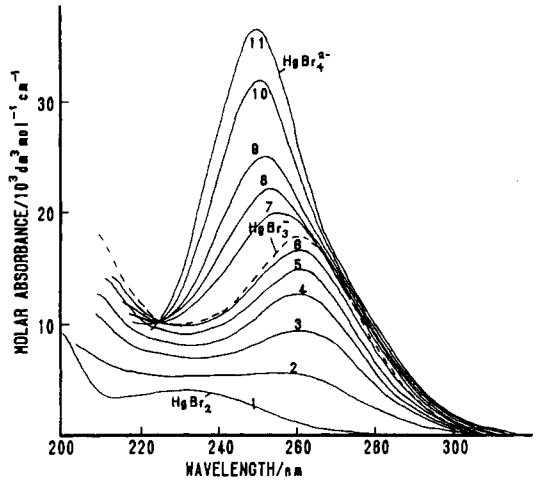


**Figure 2.** Ultraviolet absorption spectra changes obtained upon addition of bromide to $HgBr_2$ ($1.1 \times 10^{-4}$ mol dm$^{-3}$) in methanol at 20 °C. Bromide/mercury mole ratios ($R$) are, progressively (1) 2.0 ($HgBr_2$), (2) 4, (3) 20, (4) 40, (5) 90, (6) 200, (7) 800, (8) 1200, (9) 1600, (10) 20 000, and (11) 60 000 ($HgBr_4^{2-}$). Note that, compared with those of the iodide system, much greater $R$ values are required initially to produce observable changes, even though essentially the same $R$ values are needed for complete conversion to the tetrahalides. The dotted curve is the calculated spectrum of $HgBr_3^-$ in methanol. A single isosbestic point is seen at 226 nm, for the equilibrium $HgBr_3^- \rightleftharpoons HgBr_4^{2-}$.

were computed from the regression coefficients and are thus accurate and reliable.

## Results

The mercury(II) halides are readily soluble and less dissociated in methanol than in water, as was evident from studies of their spectra with respect to concentration change. Both $HgI_2$ and $HgBr_2$ obeyed the Beer–Lambert law for all concentrations used. Mercury(II) chloride obeyed the law for concentrations above $4 \times 10^{-5}$ mol dm$^{-3}$ but could not be checked at lower concentrations due to the very low absorbances involved.

**Reaction between Mercury(II) Iodide and Added Iodide. Experimental Spectra.** The changes in the spectra on addition of $I^-$ to $HgI_2$ in methanol at 20 °C (Figure 1) followed the pattern for the same system in water.[7] Initially, peaks rose at 303 and 257 nm, attributable to $HgI_3^-$, and the $HgI_2$ peak at 211 nm decreased. Isosbestic points appeared at 205 and 227 nm. As the iodide/mercury mole ratio (here termed $R$) increased to 3.0, another peak arose at 215 nm, also attributed to $HgI_3^-$. On further addition of iodide, the absorption of free iodide in methanol in the reference cell prevented observation of spectra below 250 nm (see Halide Imbalance above). The peaks at 257 and 303 nm rose slowly until $R = 10$, after which a 10-fold increase in $R$ increased the absorbance by only a few percent, showing the high stability of $HgI_3^-$ over a wide range of iodide concentrations. Between $R$ values of 100 and 1000, broadening of these peaks occurred, with a slight increase in peak height as $HgI_4^{2-}$ began to form. Thereafter, as $HgI_3^-$ was converted to $HgI_4^{2-}$, the peaks shifted to 268 and 326 nm and continued to rise, and isosbestic points appeared at 310.5 and 291.5 nm. Above $R = 20\,000$, little further change occurred, but $R > 100\,000$ was required to effect complete conversion of all the mercury present to the tetrahalide. However, there was no $R$ value, or range of values, corresponding to *only* $HgI_3^-$ in solution.

To establish that two-species equilibria existed over the appropriate ranges of $R$, the spectra were checked for internal linearity. In such circumstances, where the total concentration of metal (here mercury) remains constant, but the relative amounts of the two metal complexes changes, then a plot of absorbance at a wavelength near the maximum absorbance of one species versus that at a corresponding wavelength for the other species, i.e. at opposite sides of an isosbestic point, will give a straight line if there are only two complexes of the metal present in solution. This was found.

No attempt was made in this study to maintain solutions at constant ionic strength, partly because so doing would reduce the maximum amount of added halide that could be employed in this solvent of medium dielectric constant.

**Calculation of the Spectrum of $HgI_3^-$.** The spectrum of $HgI_3^-$ in methanol was calculated by using the reference-point method, with 11 600 ± 20 dm$^3$ mol$^{-1}$ cm$^{-1}$ at 311 nm and then with 11 340 ± 20 dm$^3$ mol$^{-1}$ cm$^{-1}$ at 292 nm, corresponding to the isosbestic points for the $HgI_3^- \rightleftharpoons HgI_4^{2-}$ equilibrium. A series of sample spectra were used in the calculation, with $R$ values of 2.2–10. In all cases, the calculated spectrum passed through *both* isosbestic points and gave peaks at 303 nm ($\epsilon$ = 12 700 ± 200 dm$^3$ mol$^{-1}$ cm$^{-1}$) and 256 nm ($\epsilon$ = 18 700 ± 300 dm$^3$ mol$^{-1}$ cm$^{-1}$). The calculated spectrum of $HgI_3^-$ is also shown in Figure 1.

Below 250 nm, the uncomplexed iodide present in methanol has a significant absorbance, causing a considerable imbalance between sample and reference cells. The $HgI_3^-$ spectrum below 250 nm therefore incorporates this correction.

As an independent check, the molar absorbance of $HgI_3^-$ at 303 nm was made by using a comparative absorbance plot, and a least-squares fit to the data yielded a value of 12 700 ± 200 dm$^3$ mol$^{-1}$ cm$^{-1}$, in good agreement with the reference-point method result.

**Calculation of the Formation Constant, $K_3$, for $HgI_3^-$.** The formation constant of $HgI_3^-$ in methanol at 20 °C was computed for a wide range of added halide concentrations. Data points at 1-nm intervals between 260 and 350 nm were used: below 260 nm, the spectra were considered not sufficiently reliable, due to the uncomplexed iodide absorption contributing to the recorded absorbance.

The formation constant $K_3$ varied continuously with ionic strength. A plot of log $K_3$ versus $I^{1/2}$ gave a straight line at low ionic strength with an intercept of log $K_3$ = 5.26 ± 0.02 at zero ionic strength. This compares well with the value of 5.24 ± 0.02 obtained from the comparative absorbance plot used to find $\epsilon$ at 303 nm.

**Reaction between Mercury(II) Bromide and Added Bromide. Experimental Spectra.** The spectral changes accompanying the reaction between $HgBr_2$ and added $Br^-$ in methanol at 20 °C are shown in Figure 2. The progressive change was different from that for the iodo system, and much greater $R$ values were needed to produce significant absorbance changes. A peak rose at 260 nm, attributed to $HgBr_3^-$, until $R = 100$, after which it shifted to lower wavelengths, and an isosbestic point appeared at 226 nm as $HgBr_4^{2-}$ formed. A corresponding point was not observed in the aqueous system.[22] The peak shift and rise continued until

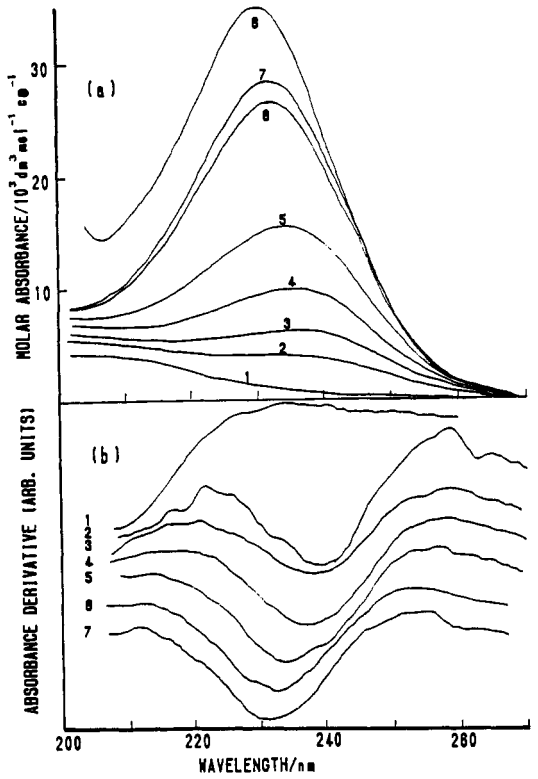


**Figure 3.** (a) Ultraviolet absorption spectra changes obtained upon addition of chloride to $HgCl_2$ ($3.8 \times 10^{-4}$ mol dm$^{-3}$) in methanol at 20 °C. Chloride/mercury mole ratios ($R$) are, progressively (1) 2.0 ($HgCl_2$), (2) 50, (3) 100, (4) 400, (5) 3000, (6) 4000, (7) 15000, and (8) 800000 ($HgCl_4^{2-}$). Higher $R$ values are required initially than in the iodo or bromo systems to produce observable changes. No isosbestic points are observed for this system. (b) Inverted fourth-derivative curves for spectra 1–7 in a, calculated by using a 13-point convolute, indicating a peak at 236 nm for $HgCl_3^-$.

$R$ reached 60000, after which this peak, now at 250 nm, did not further change, due to complete conversion of the mercury to $HgBr_4^{2-}$.

The isosbestic point at 226 nm was too close to the solution UV cutoff at 222 nm for a reliable internal linearity plot to be made, and a two-species equilibrium between $HgBr_4^{2-}$ was thus assumed for solutions where their spectra passed through this point.

**Calculation of the Spectrum of $HgBr_3^-$.** The presence of the 226-nm isosbestic point enabled the calculation of the $HgBr_3^-$ spectrum using the reference-point method. The reference point (226 nm) had an absorbance of 10270 ± 50 dm$^3$ mol$^{-1}$ cm$^{-1}$. To use this method, sample solutions containing only $HgBr_2$ and $HgBr_3^-$ were needed but were not obviously identifiable since no isosbestic points were recorded for the $HgBr_2 \rightleftharpoons HgBr_3^-$ equilibrium. Those solutions additionally containing $HgBr_4^{2-}$ were identified upon calculating the second and fourth derivation curves for a series of spectra at various $R$ values. Those derivative spectra showing no evidence of the 250-nm $HgBr_4^{2-}$ peaks were used in the subsequent calculation of the $HgBr_3^-$ spectrum: derivative spectra enhance small peaks at the expense of broad peaks and thus are excellent for identifying the presence or absence of trace quantities.[23] An $R$ value of <100 was found necessary, and from these spectra the spectrum of $HgBr_3^-$ with a single peak at 260 nm ($\epsilon$ = 17800 ± 300 dm$^3$ mol$^{-1}$ cm$^{-1}$) was derived (Figure 2). This was independently confirmed by a comparative absorbance plot at 260 nm, which gave a molar absorbance of 17700 ± 200 dm$^3$ mol$^{-1}$ cm$^{-1}$, well within experimental error. The halide imbalance was included in the calculation of the $HgBr_3^-$ spectrum but was not significant over the spectral range used, as the bromide ion in methanol only absorbs appreciably below 220 nm.

(22) Griffiths, T. R.; Anderson, R. A. Unpublished results.
(23) Griffiths, T. R.; King, K.; Hubbard, H. V. St. A.; Schwing-Weill, M.-J.; Meullemeestre, J. *Anal. Chim. Acta* **1982**, *143*, 163.

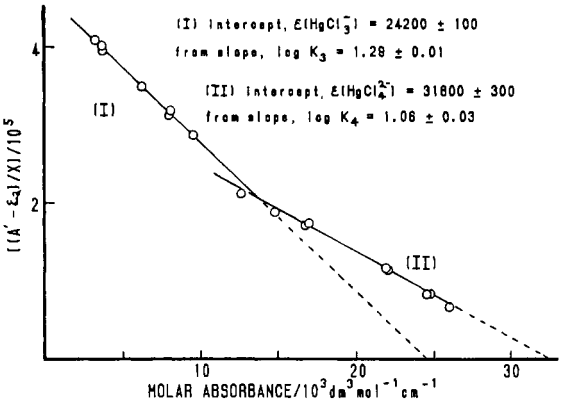


**Figure 4.** Comparative absorbance plot, employing 16 different $R$ values, for $HgCl_2$ in methanol at 20 °C with added chloride, using absorbance data at 236 nm in eq 6. I corresponds to the equilibrium $HgCl_2 + Cl^- = HgCl_3^-$, and the value of the intercept for $\epsilon(HgCl_3^-)$ at 236 nm is required in order to calculate the complete spectrum of $HgCl_3^-$ by the reference-point method. II corresponds to the equilibrium $HgCl_3^- + Cl^- = HgCl_4^{2-}$, and the value of $\epsilon(HgCl_4^{2-})$ at 236 nm so determined is within experimental error of that recorded for $HgCl_4^{2-}$ in Figure 3a.

**Calculation of the Formation Constant, $K_3$, for $HgBr_3^-$.** The formation constant for $HgBr_3^-$ in methanol at 20 °C was computed using data points at 1-nm intervals. Absorbance values between 220 and 300 nm were used for solutions containing only $HgBr_2$ and $HgBr_3^-$ and values between 240 and 300 nm for solutions containing only $HgBr_3^-$ and $HgBr_4^{2-}$. The value of log $K_3$ was constant (3.08 ± 0.08) at ionic strengths below $2.5 \times 10^{-3}$ mol dm$^{-3}$, but decreased as the concentration of bromide was further increased. This compares well with log $K_3$ = 3.03 ± 0.02, obtained from the comparative absorbance plot at 260 nm, where the ionic strength maximum was around $1 \times 10^{-3}$ mol dm$^{-3}$.

**Reaction between Mercury(II) Chloride and Added Chloride. Experimental Spectra.** This reaction in methanol at 20 °C is illustrated in Figure 3a. This set of spectra evinces no isosbestic point. On the $HgCl_2$ peak, at 204 nm ($\epsilon$ = 4000 ± 100 dm$^3$ mol$^{-1}$ cm$^{-1}$), a shoulder arises on the long-wavelength edge, forming into a peak at 236 nm as $HgCl_3^-$ is formed. This peak then broadened as $HgCl_4^{2-}$ was also produced, ultimately narrowing to a peak at 230 nm ($R$ = 800000), when all the mercury present was in the form $HgCl_4^{2-}$. Due to differing solubilities, with $HgCl_2$ concentrations of $(2–4) \times 10^{-4}$ mol dm$^3$, KCl was unsable up to $R \sim 1000$ and $NH_4Cl$ with $R$ up to ~15000, and higher $R$ values were obtained with use of LiCl.

**Calculation of the Spectrum of $HgCl_3^-$.** Our options for this system were reduced, since isosbestic points were not observed. Fourth-derivative curves of a series of spectra of solutions with $R$ between 2 and 15000 showed a peak at 236 nm, for $HgCl_3^-$ (Figure 3b). A comparative absorbance plot at 236 nm gave the molar absorbance of $HgCl_3^-$ at this wavelength as 24200 ± 200 dm$^3$ mol$^{-1}$ cm$^{-1}$ (Figure 4). This value, used in the reference-point method, enabled the complete spectrum of $HgCl_3^-$ to be calculated from a series of spectra. This calculated spectrum had a peak at 236 nm ($\epsilon_{max}$ = 24200 ± 200 dm$^3$ mol$^{-1}$ cm$^{-1}$) and had a similar consistency (within ±300 dm$^3$ mol$^{-1}$ cm$^{-1}$) over the whole spectral range (Figure 5).

**Calculation of the Formation Constant, $K_3$, for $HgCl_3^-$.** The formation constant of $HgCl_3^-$ in methanol at 20 °C was computed by using data points at 1-nm intervals over the range 205–260 nm. A plot of log $K_3$ versus $I^{1/2}$ showed $K_3$ constant at low ionic strengths, with log $K_3$ = 1.28 ± 0.01, but decreasing above $7 \times 10^{-2}$ mol dm$^{-3}$. This compares well with log $K_3$ = 1.29 ± 0.01 obtained from the comparative absorbance plot at 236 nm (Figure 4).

## Discussion

Having established, for the first time, the electronic absorption spectra of $HgI_3^-$, $HgBr_3^-$, and $HgCl_3^-$ in methanol, and having noted that their profiles are not all similar, we were prompted to investigate their structures in solution. We have therefore resolved

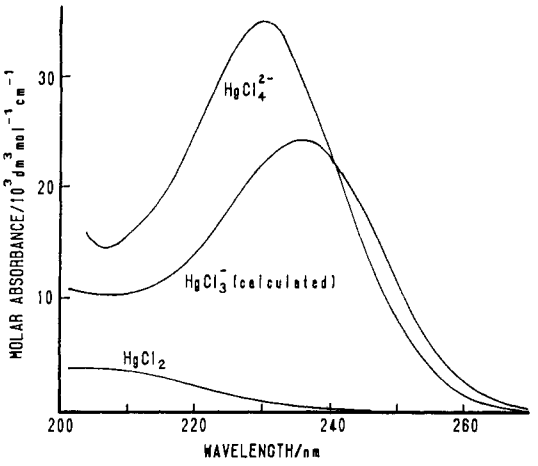


**Figure 5.** Plot of the calculated electronic spectrum of $HgCl_3^-$ in methanol at 20 °C, compared with the spectra of $HgCl_2$ and $HgCl_4^{2-}$. Although the spectra of $HgCl_3^-$ and $HgCl_4^{2-}$ cross, indicating that as $R$ is increased for this equilibrium reaction, an isosbestic point might be seen: in practice, because they cross at a shallow angle, a definitive isosbestic point cannot be observed experimentally, as indicated in Figure 3a.

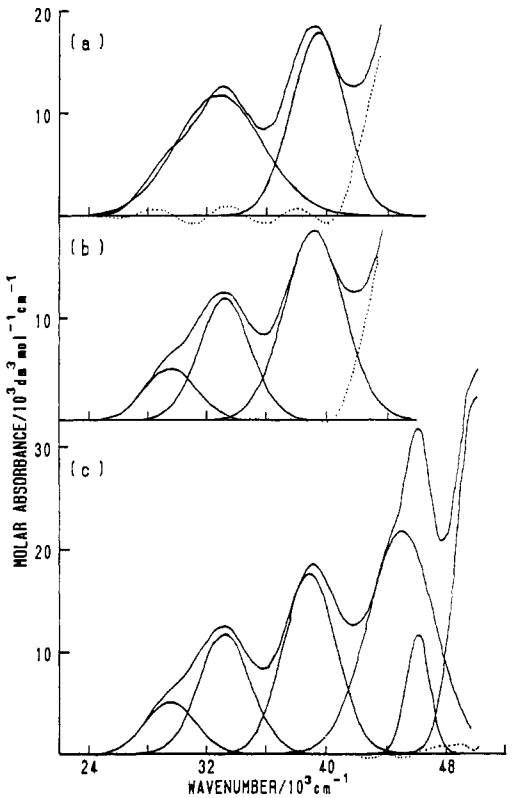


**Figure 6.** Gaussian analysis of the calculated spectrum of $HgI_3^-$: (a) analysis for two Gaussian bands using data points up to 40 000 $cm^{-1}$ (dotted line is the difference between the sum of the best fit of the Gaussian curves and the calculated spectrum of $HgI_3^-$; (b) analysis up to 40 000 $cm^{-1}$; (c) best overall fit, using all available data points, which employs six Gaussian bands and includes a peak at 217 nm (see text).

each spectrum into its component Gaussian bands and then derived their associated structure using Walsh diagrams.[24]

**Analysis of the Spectra of the Trihalides.** Our procedures have been described in detail elsewhere.[12] Derivative spectra[23] were first calculated to determine the number of bands under the profile. For $HgI_3^-$, the low-energy band revealed at around 340 nm is not a clear shoulder in the original, zero-derivative spectrum. This band was confirmed upon Gaussian analysis (using that part of the spectrum not affected by the halide imbalance correction

(24) Walsh, A. D. *J. Chem. Soc.* **1953**, 2266 and subsequent papers.

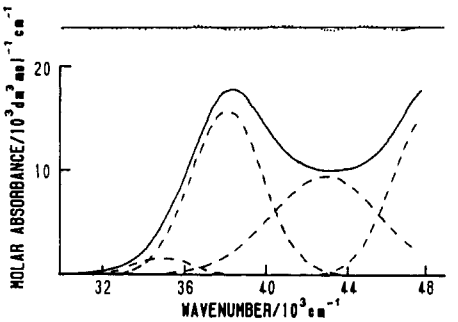


**Figure 7.** Gaussian analysis of the calculated spectrum of $HgBr_3^-$ for four bands, using all available data points. Dotted line is the difference between the sum of the Gaussian curves and the calculated spectrum of $HgBr_3^-$.

**Table I.** Absorption Band Parameters[a] for $HgX_3^-$ in Methanol at 20 °C

| | obsd peaks | | resolved bands | | | | |
|---|---|---|---|---|---|---|---|
| species | $E_{max}$ | $\epsilon_m$ | $E_{max}$ | $\epsilon_m$ | $\omega$ | $A$ | OS |
| $HgI_3^-$ | | | 29.50 | 5130 | 3.98 | 4.35 | 1.88 |
| | 33.11 | 12520 | 33.19 | 11780 | 4.11 | 10.4 | 4.49 |
| | 39.06 | 18590 | 38.92 | 17950 | 4.11 | 15.7 | 6.78 |
| | 46.08 | 32230 | 45.00 | 22000 | 5.26 | 24.7 | 10.7 |
| | | | [46.10 | 12000 | 1.86 | 4.75 | 2.05][b] |
| | | | 50.00 | 35000 | 3.03 | 22.6 | 9.76 |
| $HgBr_3^-$ | | | 35.00 | 1600 | 3.32 | 1.13 | 0.49 |
| | 38.46 | 17820 | 38.16 | 15800 | 4.15 | 13.9 | 6.00 |
| | | | 43.00 | 9600 | 6.28 | 12.9 | 5.57 |
| | | | 48.10 | 15800 | 4.15 | 13.9 | 6.00 |
| $HgCl_3^-$ | 42.37 | 24280 | 42.05 | 20000 | 4.03 | 17.2 | 7.43 |
| | | | 45.50 | 11500 | 5.53 | 13.6 | 5.87 |

[a] $E_{max}$ = peak maximum ($10^3$ $cm^{-1}$); $\epsilon_m$ = molar absorbance ($dm^3$ $mol^{-1}$ $cm^{-1}$); $\omega$ = bandwidth at half-height ($10^3$ $cm^{-1}$); $A$ = band area ($10^{-4}$ $dm^3$ $mol^{-1}$ $cm^{-1}$); OS = oscillator strength. [b] See text and Figure 6.

applied in the calculation of the $HgI_3^-$ spectrum), which gave a poor fit for only two bands (Figure 6a) but a good fit if another band at about 340 nm was included (Figure 6b). The rising absorbance below 210 nm (Figure 1) also indicated the need to include the contribution of a band at high energy. The best overall fit was obtained upon Gaussian analysis for six bands (Figure 6c), which includes a band at 217 nm. However, this peak is close to that known for the charge transfer to solvent transition of the iodide ion in methanol (218 nm), and since it has no analogue in the spectrum of $HgI_3^-$ in water,[7] it is currently omitted in the molecular orbital scheme. It could thus arise if the halide imbalance correction could not be made with sufficient accuracy to eliminate completely the absorbance contribution from free iodide in the sample spectra.

In the case of $HgBr_3^-$ in methanol, derivative spectra also revealed a band hidden on the low-energy side of the observed peak. When this band was included in the Gaussian analysis of the spectrum, a good fit for four bands was obtained (Figure 7).

The bands present in the spectrum of $HgCl_3^-$ corresponded to one main spectral peak and a second band at higher energy. No evidence for hidden peaks in the main band was found by derivative analysis. The contribution of a third band at yet higher energies could be deduced from the spectrum, but could not be computed with any accuracy, and thus no estimate could be obtained for its peak maximum.

The parameters for the observed peaks and resolved bands are given in Table I.

**Interpretation of the Spectra of the Trihalides.** The trihalogenomercurates may have a pyramidal or planar structure, corresponding to $C_{3v}$ and $D_{3h}$ symmetry, respectively. The order of the molecular orbitals, after Walsh,[24] is given in Figure 8a for $MX_3$ molecules, of structures from planar to pyramidal. The $HgX_3^-$ species have 24 valency electrons, and these will fill the orbitals up to and including $1a_2$. The $(1a_2)^2$ ground state for both planar and pyramidal molecules is $^1A_1$. In $C_{3v}$ symmetry, the

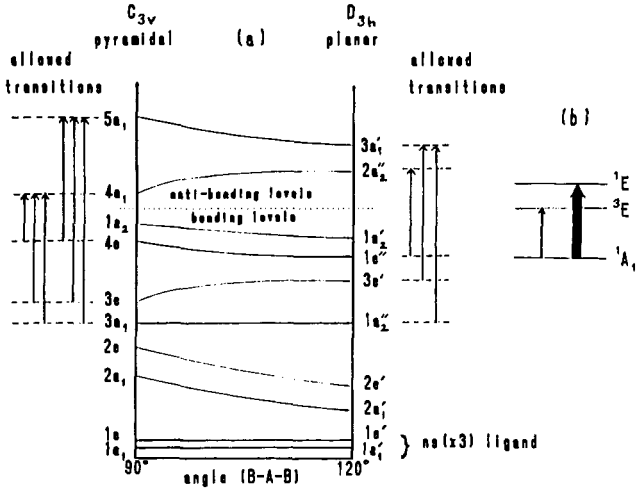


**Figure 8.** (a) Correlation diagram for the orbitals of $AB_3$ molecules with $D_{3h}$ and $C_{3v}$ symmetry; (b) spin-forbidden transitions made partially allowed (see text).

following electron excitations are allowed: $a_1 \leftrightarrow a_1$, $a_2 \leftrightarrow a_2$, $a_2 \leftrightarrow e$, $e \leftrightarrow e$, and $e \leftrightarrow a_1$. In $D_{3h}$ symmetry, the following are allowed: $a_1' \leftrightarrow a_2''$, $a_1' \leftrightarrow e'$, $a_2' \leftrightarrow a_1''$, $a_2' \leftrightarrow e'$, $a_1'' \leftrightarrow e''$, $a_2'' \leftrightarrow e''$, $e' \leftrightarrow e''$, $e' \leftrightarrow e'$, and $e'' \leftrightarrow e''$. The transitions relating to $HgX_3^-$ are included in Figure 8a. Excitation to the $4a_1$–$2a_2''$ orbital would favor a pyramidal excited state, whereas excitation to the $5a_1$–$3a_1'$ orbital would favor a planar configuration.

Solvation of the mercury(II) halides increases from $HgI_2$ to $HgCl_2$, as the size of the halogen atoms decreases. Addition of a halide ion to $[HgX_2(solvent)_4]^0$ to form trigonal bipyramidal $[HgX_3(solvent)_2]^-$ will occur more readily for a strongly solvated molecule with large halogen atoms. For large ligands and weak solvation, a more stable configuration would be pyramidal, with one solvent molecule occupying the fourth tetrahedral position. This solvation argument is not definitive since solvation in methanol is less understood than in water, but it is reasonably concluded that $HgI_3^-$ may be expected to be pyramidal and $HgCl_3^-$ planar. The structure of $HgBr_3^-$ will become clearer once band assignments have been made.

**Band Assignments.** Of the five transitions in the band structure of $HgI_3^-$, those at 33 190, 38 920, and 45 000 $cm^{-1}$ are assigned to the electron excitations to the $4a_1$ orbital from the 4e, 3e, and $3a_1$ orbitals, respectively. The lowest excitation, $4e \rightarrow 4a_1$, corresponds to the transition $^1A_1 \rightarrow {}^1E$. The corresponding spin-forbidden transition, $^1A_1 \rightarrow {}^3E$, of this configuration is made partially allowed by the mixing of the $^3E$ and $^1E$ states via spin–orbit coupling and gives a small low-energy peak at 29 500 $cm^{-1}$, as indicated in Figure 8b. The high-energy band at 50 000 $cm^{-1}$ is probably due to excitation from the 4e orbital to $5a_1$.

An alternative explanation for the $HgI_3^-$ spectrum is theoretically possible. Excitation of an electron from the 4e orbital to the $4a_1$ orbital (for $C_{3v}$) gives rise to the transition $^1A_1 \rightarrow {}^3E$, a spin-allowed transition. Spin–orbit coupling causes this $^1E$ state to mix with the $^3E$ state of the same configuration, which leads to splitting of $^3E$ into $A_1$, $A_2$, and two E states. For a small spin–orbit coupling (as in $HgBr_3^-$) only two transitions could be seen, but for large coupling (as expected for $HgI_3^-$) spin-forbidden transitions to E, E, and $A_1$ would lead to three bands in addition to the spin-allowed transition to $^1E$ (Figure 8b).

However, such an explanation requires that the three low-energy bands are spin-forbidden and of low intensity. Transitions to the two E states would also lead to similar intensities for the two lowest energy bands. This is not observed, since the lowest band, at 29 500 $cm^{-1}$, has a molar absorbance of 5130 $dm^3\ mol^{-1}\ cm^{-1}$ while the second band at 33 190 $cm^{-1}$ has a higher molar absorbance of 11 870 $dm^3\ mol^{-1}\ cm^{-1}$. The band at 29 500 $cm^{-1}$ is thus here considered to be spin-forbidden and the other an allowed transition, and the former explanation is therefore preferred.

The spectrum of $HgCl_3^-$ is very different from that of $HgI_3^-$, is not simply due to a blue shift, and has none of its complexities. The band structure is best explained in terms of a planar structure with $D_{3h}$ symmetry. The excitation $1e'' \rightarrow 2a''_2$, corresponding to $4e \rightarrow 4a_1$ in $C_{3v}$ symmetry, is allowed and explains the observed intense band: this is the $^1A_1 \rightarrow {}^1E'$ transition. Spin–orbit coupling is now much less strong, and coupling of the $^3E'$ state with $^1E'$ is thus not expected to be seen. The two other excitations, to $2a''_2$ from 3e′ and $1a''_2$ (corresponding to those from 3e and $3a_1$ to $4a_1$ in $HgI_3^-$), are forbidden in $D_{3h}$ symmetry and are not observed. The additional band noted at high energies is thus now thought probably due to the transition $3e' \rightarrow 3a_1'$ ($^1A_1 \rightarrow {}^1E'$). It is much wider than the main band, and this is expected for excitation to a higher antibonding orbital.

The spectrum of $HgBr_3^-$ in methanol appears initially to resemble that of $HgCl_3^-$ (Figures 2 and 5), but on consideration of the resolved bands (Table I) we find that the data are adequately explained by assuming a pyramidal structure with $C_{3v}$ symmetry. The resolved structure of the $HgBr_3^-$ spectrum consists of four bands. These bands are here identified, as in $HgI_3^-$, as excitation from the 4e, 3e, and $3a_1$ orbitals to the $4a_1$ orbital. The first main transition is thus $^1A_1 \rightarrow {}^1E$. The low-energy band, not seen in the spectrum of $HgBr_3^-$ in water,[7] arises from the spin–orbit coupling of the $^1E$ state and the $^3E$ state of the $(4e)^3(4a_1)^1$ excited state.

Sandström and Johansson[10] have reported X-ray diffraction studies for concentrated aqueous solutions of $HgBr_3^-$ and $HgI_3^-$, which indicated pyramidal structures, probably with one coordinated water molecule. While this conveniently supports our interpretation of our spectra of these species in the protic solvent methanol, we would point out that the concentrations they used were much in excess of ours and they used $R < 4$. Sandström[5] has also examined dimethyl sulfoxide (DMSO) solutions by X-ray diffraction, which indicated a planar structure for $HgCl_3^-$, probably with two interacting DMSO solvent molecules giving overall trigonal-bipyramidal coordination.

Waters et al.[2] have noted an interesting feature of $HgCl_3^-$ and $HgBr_3^-$ in amide solvents, namely, the presence of two configurational isomers, one of $D_{3h}$ symmetry (considered unsolvated) and the other possessing essentially $C_{3v}$ symmetry (having one coordinated solvent molecule). The Raman spectra also show that at $R = 3$ only the trispecies is present. The two isomers were in equilibrium, and their Raman spectra showed an isosbestic point as the temperature was changed. In this case, a study of $HgI_3^-$ would be informative, as would further work by us to expand in Table I the resolved band parameters as a function of temperature, to see if this phenomenon persists in methanol solutions: X-ray diffraction studies probably do not have sufficient precision to follow this equilibrium.

We therefore conclude that, in methanol, $HgI_3^-$ is essentially a tetrahedral species and $HgBr_3^-$ a distorted-tetrahedral species, both with one methanol molecule coordinated to mercury. For $HgCl_3^-$, the four atoms are largely coplanar, and two methanol molecules are additionally coordinated, one above and one below the plane, producing essentially a trigonal-bipyramidal species. We do not, however, find any evidence within our results for the coexistence in solution of two structurally distinct forms of (monomeric) trihalogenomercurate(II) ions in equilibrium. We note that Waters et al.[2] only investigated $HgBr_3^-$ and $HgCl_3^-$, species which in solution have structures with more potential for existing in two distinct forms than the tetrahedrally based $[HgI_3(solvent)]^-$ species, where we would anticipate that this equilibrium would not be observed. The equilibrium may also be limited to dipolar aprotic solvents, possibly just amide solvents having high dielectric constants and moderately strong coordinating powers, which type they used: protic solvents, especially those that exchange coordinated solvent molecules rapidly with the bulk solvent, may not facilitate this equilibrium. Further absorption spectra (and Raman) studies as a function of temperature in both protic and dipolar aprotic solvents should be informative.

However, we remark that Raman and X-ray studies currently employ concentrated solutions while our $HgX_3^-$ spectra were obtained at concentrations several orders of magnitude lower.

Thus, structures deduced in concentrated solutions will reflect the effects of contiguous counterions. Enderby[25] has for example reported neutron scattering studies on concentrated aqueous nickel(II) chloride solutions and found that the angle between the nickel ion and the oxygen atom on the coordinated water molecules and the line bisecting the water protons decreases from 180° with concentration increase above about 0.1 mol $dm^{-3}$. The maximum angle of tilt from 180°, which he observed at 42 ± 8° for solutions in excess of about 1.0 mol $dm^{-3}$, is not, in our view, due to hydrogen bonding but the effect of the neighboring chloride ions. In his most concentrated solutions, around 4 mol $dm^{-3}$, the average separation between nickel and chloride ions is about 5 Å, and thus these ions are competing for the same water molecule in their solvation shells.

**Acknowledgment.** We thank the SERC for the provision of the Cary 14H spectrophotometer. The digitizing equipment was purchased on Harwell Contract EMR 1913. R.A.A. thanks the University of Leeds for a postgraduate research grant; T.R.G. thanks the University of Leeds and the Province of Alberta, Canada, for a travel grant under their Leeds-Alberta Link Scheme, and the Chemistry Department, University of Calgary, for hospitality and facilities during the preparation of this paper.

**Registry No.** $HgCl_3(MeOH)_2^-$, 132751-00-9; $HgBr_3(MeOH)^-$, 132751-01-0; $HgI_3(MeOH)^-$, 132751-02-1.

(25) Enderby, J. E. *Sci. Prog.* **1981**, *67*, 553.

Contribution from the Department of Chemistry, Rensselaer Polytechnic Institute, Troy, New York 12180-3590, Department of Physics, University of Pennsylvania, Philadelphia, Pennsylvania 19104-6396, and General Electric Corporate Research and Development, Schenectady, New York 12301

# Comparison of Isoelectronic Aluminum-Nitrogen and Silicon-Carbon Double Bonds Using Valence Bond Methods

Mary M. Lynam,[†] Leonard V. Interrante,[†] Charles H. Patterson,[‡,§] and Richard P. Messmer*[,⊥]

*Received January 16, 1990*

In the reaction between trimethylaluminum and ammonia to form aluminum nitride, $(CH_3)_2AlNH_2$ is a postulated intermediate. Results of ab initio geometry optimization calculations for this species as well as $H_2AlNH_2$ and isoelectronic $H_2SiCH_2$ are presented. Each of these has a planar equilibrium skeleton with $C_{2v}$ symmetry. Geometry optimizations were carried out by using generalized valence bond (GVB) wave functions. Al=N bond distances of 1.78 and 1.80 Å are predicted for the dihydro- and dimethylaluminum amides, respectively, which are slightly longer than the optimized Si=C bond distance of 1.74 Å in $H_2SiCH_2$. Al=N bond distances in these compounds are found to agree with a phenomenological correlation established by Haaland, which relates the ratio of covalent to dative character of such bonds to the observed bond distances. We compare the bonding in Al=N and Si=C molecules by analyzing the nature of the GVB orbitals describing the bonds and comparing their predicted dipole moments.

## Introduction

Oligomeric alkylaluminum amides[1-9] $(R_2AlNR'R'')_n$ have recently been the subject of renewed interest owing to their potential utility as precursors to aluminum nitride[8,10,11] (AlN). As described in the review by Bahr,[12] E. Wiberg in 1939 elucidated a series of reactions involving the synthesis of methylaluminum amides and imides, which generate aluminum nitride when heated:

$$Me_3Al + NH_3 \rightarrow Me_3Al{\cdot}NH_3 \rightarrow (Me_2AlNH_2)_{2\text{ or }3} \rightarrow (MeAlNH)_n \rightarrow AlN \quad (I)$$

The rational design of precursors to aluminum nitride requires a detailed knowledge of the intermediate steps that occur in the sequence of reactions in (I); in particular, in this work we are interested in the first methane loss step, which results in formation of aluminum amides. Interrante et al.[8] have studied the thermodynamic, kinetic, and mechanistic aspects of the reaction

$$Me_3Al + NH_3 \rightarrow Me_3Al{\cdot}NH_3 \rightarrow \tfrac{1}{3}(Me_2AlNH_2)_3 + CH_4 \quad (II)$$

and have proposed monomeric $Me_2AlNH_2$ as an intermediate that participates as a catalyst in methane loss from the Lewis acid-base adduct $Me_3Al{\cdot}NH_3$.[9] This species may also be present as a gas phase or surface-adsorbed species in the chemical vapor deposition of AlN[13] and in solution during the thermal equilibration of the more thermodynamically stable trimeric species $(Me_2AlNH_2)_3$.[14] The theoretical studies reported here pursue the question of the structure and bonding in $Me_2AlNH_2$. We compare bonding and the predicted structure of $Me_2AlNH_2$ to those of two related molecules—$H_2AlNH_2$, and $H_2SiCH_2$.

The strong tendency of alkylaluminum amides to oligomerize results in formation of Lewis acid-base complexes of the type $(R_2AlNR'R'')_n$ whose structures consist of four- or six-membered aluminum-nitrogen rings whose size ($n$ = 2 or 3) depends largely on the particular groups attached to Al or N. Heating the aluminum amides to moderate temperatures in solution results in elimination of alkane and formation of alkylaluminum imides $(RAlNR')_n$.[15-17] Imide aggregates with $n$ up to 16 have been

† Rensselaer Polytechnic Institute.
‡ University of Pennsylvania.
§ Present address: Department of Pure and Applied Physics, University of Dublin, Trinity College, Dublin 2, Ireland.
⊥ General Electric Corporate Research and Development.

(1) Atwood, J. L.; Stucky, G. D. *J. Am. Chem. Soc.* **1970**, *92*, 287.
(2) McLaughlin, G. M.; Sim, G. A.; Smith, J. D. *J. Chem. Soc., Dalton Trans.* **1972**, 2197.
(3) Semenko, K. N.; Loblouski, E. B.; Dovsinskii, A. L. *J. Struct. Chem. (Engl. Transl.)* **1972**, *13*, 696.
(4) Lappert, M. F.; Power, P. P.; Sanger, A. R.; Srivastava, R. C. *Metalloid Amides*; Ellis Horwood: Chichester, England, 1980.
(5) Amirkhalili, S.; Hitchcock, P. B.; Jenkins, A. D.; Nyathi, J.; Smith, J. D. *J. Chem. Soc., Dalton Trans.* **1981**, 377.
(6) Interrante, L. V.; Carpenter, L. E.; Whitmarsh, C.; Lee, W.; Slack, G. A. *Mater. Res. Soc. Symp. Proc.* **1986**, *73*, 986.
(7) Janik, J. F.; Duesler, E. N.; Paine, R. T. *Inorg. Chem.* **1987**, *26*, 4341.
(8) Interrante, L. V.; Sigel, G. A.; Garbauskas, M.; Hejna, C.; Slack, G. A. *Inorg. Chem.* **1989**, *28*, 252.
(9) Sauls, F. C.; Interrante, L. V.; Jiang, Z. *Inorg. Chem.* **1990**, *29*, 2989.
(10) Bolt, J. D.; Tebbe, F. N. Aluminum Nitride Fibers: Sintering and Microstructure. *Proc. Am. Ceram. Soc. Electron. Div.* **1987**, Oct 19.
(11) Tebbe, F. N.; Bolt, J. D.; Young R. J.; Van Buskirk, O. R.; Mahler, W.; Reddy, G. S.; Chowdry, U. Thermoplastic Organoaluminum Precursors of Aluminum Nitride. *Proc. Am. Ceram. Soc. Electron. Div.* **1987**, Oct 19.
(12) Bahr, G. In *Inorganic Chemistry, part II: FIAT Review of WWII German Science*; Klemm, W., Ed.; Dieterichsche Verlagsbuchhandlung: Wiesbaden, Germany, 1948; Vol. 24, p 155.
(13) Interrante, L. V.; Lee, W.; McConnell, M.; Lewis, N.; Hall, E. *J. Electrochem. Soc.* **1989**, *132*, 472. Hanson, S. A.; Evans, J. F.; Boyd, D. C.; Gladfelter, W. L.; Ho, K. L.; Jesnen, K. V. Presentation at the 36th National American Society Meeting, Boston, MA, Oct 23-27, 1989; see Abstract No. TF-THM2.
(14) Sauls, F. C.; Czekaj, C. L.; Interrante, L. V. *Inorg. Chem.* **1990**, *29*, 4688.
(15) Wiberg, E.; May, A. *Z. Naturforsch.* **1955**, *B10*, 232.

0020-1669/91/1330-1918$02.50/0 